RSC Advances

PAPER

View Article Online
View Journal | View Issue

Cite this: *RSC Adv.*, 2018, **8**, 38648

Simultaneous adsorption of SO_2 and CO_2 in an Ni(bdc)(ted)$_{0.5}$ metal–organic framework†

Do Ngoc Son, *[a] Ta Thi Thuy Huong[a] and Viorel Chihaia [b]

Received 24th September 2018
Accepted 5th November 2018

DOI: 10.1039/c8ra07919f

rsc.li/rsc-advances

The metal–organic framework Ni(bdc)(ted)$_{0.5}$ is a promising material for simultaneous capture of harmful gases such as SO_2 and CO_2. We found that SO_2 performs much better than CO_2 during adsorption, and the lack of physical insight was clarified through detailed analyses of the electronic structures obtained from density functional theory calculations. Our results showed that strong interactions of the d band of Ni atoms with the valence states (2n, 3n, and 4n) of SO_2 but almost not with those of CO_2 are the main reasons. Our finding is useful for the rational design of new metal–organic frameworks with suitable interactions for the simultaneous capture of not only SO_2 and CO_2 but also other gases.

I. Introduction

CO_2 is a greenhouse gas leading to global warming, and SO_2 is the primary source of acid rain.[1,2] With increasing consumption of fossil fuel energies, emissions of SO_2 and CO_2 are becoming more serious. The removal of these gases is, therefore, an active research area attracting much attention from scientists. Among the proposed materials and techniques,[3–6] metal–organic frameworks (MOFs) are the most promising candidates that satisfy the practical requirements of high stability, high gas uptake capacity, low energy of gas desorption, and low cost.

Due to exceptionally high surface area, tunable porous crystals, and structural versatility, MOFs exhibit excellent ability for the capture and selective separation of a wide range of gases based on adsorption.[7] Particularly, MOF-200 and MOF-210 have shown the highest CO_2 uptake so far up to more than 70 wt%.[8] Several studies have also been devoted to the study of SO_2 capture using MOFs.[6,9–14] Because of the co-existence of SO_2 and CO_2 in the same practical environment and the need for the removal of these gases to mitigate their influences on the climate, the simultaneous capture of the gases within the same MOF is particularly important.[6,15–18] Recently, Tan and coworkers found that Ni(bdc)(ted)$_{0.5}$ (bdc = benzenedicarboxylate, ted = triethylenediamine) can adsorb a significant amount of SO_2 (9.97 mmol g^{-1}) and simultaneously exhibit remarkable uptake of CO_2 at low pressure and ambient temperature.[13,19,20] Remarkably, SO_2 performs much better than CO_2 during co-adsorption by Ni(bdc)(ted)$_{0.5}$ as SO_2 can replace pre-adsorbed CO_2;[13] however, the physical insights into this phenomenon remain unexplained.

Here, we used van der Waals-corrected density functional theory,[21–24] which has been successfully applied in previous studies,[25–27] to reveal the electronic nature of MOF-gas interactions. Thus, our study is necessary, and the current findings are useful for the design of new MOFs for simultaneous adsorption of other gases.

II. Computational details

Density functional theory calculations were performed using the Vienna Ab Initio Simulation Package. The exchange and correlation functionals[21,28] including the van der Waals dispersion corrections, vdW-DF,[22,29] were used in this study. The electron-ion interactions were described by the projector augmented-wave method[23,24] with a plane wave cut-off of 700 eV. The integration over the Brillouin zone was calculated using the Monkhorst–Pack scheme[30] with k-point sampling of $5 \times 5 \times 5$ for geometry optimization and electronic structure calculations. The size and shape of the unit cell of Ni(bdc)(ted)$_{0.5}$ were fully optimized; it exhibited a tetragonal structure with cell parameters of $a = b = 11.15$ Å and $c = 9.53$ Å (Fig. 1).[13] Spin polarization was performed for geometry optimization and total energy calculation.

The adsorption energy E_{ad} is defined as follows:

$$E_{ad} = E_{MOF+SO_2/CO_2} - E_{MOF} - E_{SO_2/CO_2}. \quad (1)$$

Here, E_{MOF+SO_2/CO_2}, E_{MOF}, E_{SO_2}, and E_{CO_2} are the total energies of the MOF + gas system, MOF Ni(bdc)(ted)$_{0.5}$, isolated SO_2, and isolated CO_2, respectively.

The charge density difference[31–33] was calculated for the most stable configurations of the adsorbed SO_2 and CO_2 using the following formula:

[a]University of Technology, VNU-HCM, 268 Ly Thuong Kiet Street, District 10, Ho Chi Minh City, Vietnam. E-mail: dnson@hcmut.edu.vn

[b]Institute of Physical Chemistry "Ilie Murgulescu" of the Romanian Academy, Splaiul Independentei 202, Sector 6, 060021 Bucharest, Romania

† Electronic supplementary information (ESI) available: Molecular orbital diagrams for SO_2 and CO_2. See DOI: 10.1039/c8ra07919f

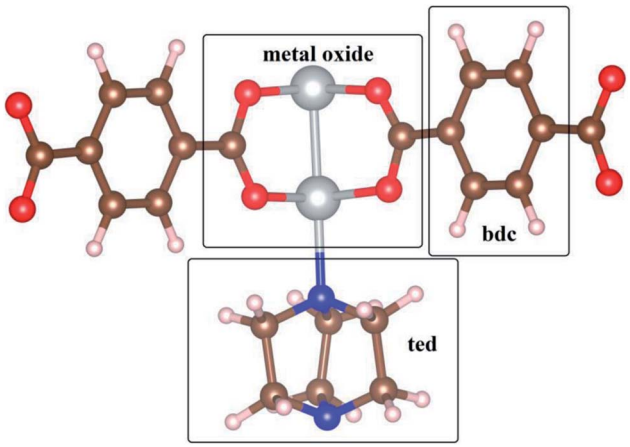

Fig. 1 The unit cell of Ni(bdc)(ted)$_{0.5}$; C (brown), O (red), H (white), N (blue), and Ni (silver).

$$\Delta\rho = \rho_{MOF+SO_2/CO_2} - \rho_{MOF} - \rho_{SO_2/CO_2}. \quad (2)$$

Here, ρ_{MOF+SO_2/CO_2} and ρ_{MOF} are the charge densities of the MOF + gas system and MOF Ni(bdc)(ted)$_{0.5}$, respectively; ρ_{SO_2} and ρ_{CO_2} are the charge densities of the single molecule SO_2 and CO_2, respectively. Here, the charge density of the MOF and the gas was calculated from the corresponding structures obtained from the MOF + gas system by removing either the gas or the MOF, respectively.

The partial point charges for each atom of SO_2 and CO_2 and MOF were estimated using the Bader charge partition method.[34,35]

III. Results and discussion

We label the unit cell surface of Ni(bdc)(ted)$_{0.5}$ by three main regions: bdc, ted, and metal oxide (Fig. 1). For single gas adsorption, we load each molecule of SO_2 and CO_2 to various positions on the surface of Ni(bdc)(ted)$_{0.5}$. We then optimize the geometry and calculate the adsorption energy of SO_2 and CO_2. We select the most stable configuration of SO_2 and CO_2 in each surface region based on the obtained adsorption energy, as presented in Fig. 2, for further analyses. This figure also exhibits the bond distances between SO_2 and CO_2 with the nearest atoms of Ni(bdc)(ted)$_{0.5}$. To roughly understand the nature of MOF-gas interaction, we analyze the bond distance between the gas and the MOF. In this study, the atomic radii are defined through the Wigner–Seitz radius, which are 0.37, 0.741, 0.783, 0.863, 0.953, and 1.286 Å for H, O, N, C, S, and Ni, respectively. Generally, the length of a covalent bond between two atoms equals the sum of the radii of the two atoms. If there are covalent bonds, the standard bond lengths of C–S, O–H, S–O, C–C, and C–O between the gas and MOF, as shown in Fig. 2, are expected to be 1.816, 1.111, 1.694, 1.726, and 1.602 Å, respectively. However, the nearest bond distances (Fig. 2) are much longer than these standard covalent bond lengths. Therefore, there is physical interaction rather than a covalent bond between the gases and MOF.

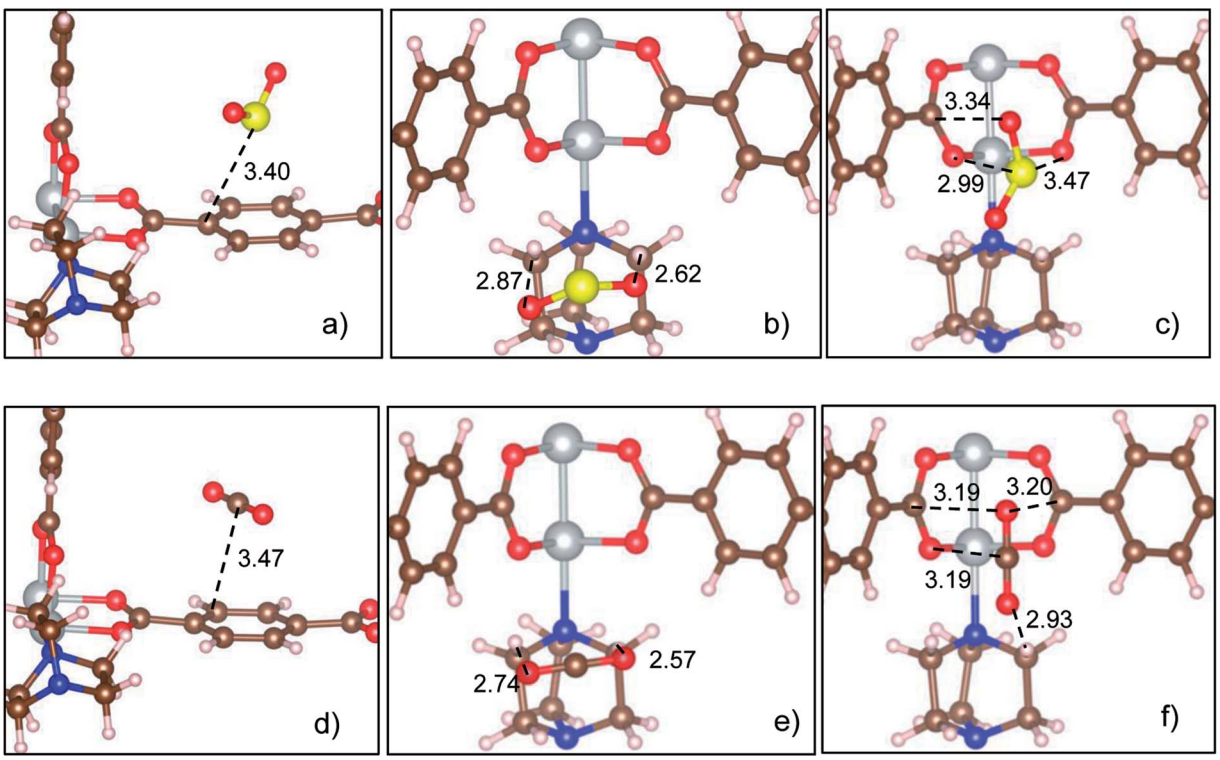

Fig. 2 Stable adsorption configurations of SO_2 (upper panel) and CO_2 (lower panel) on bdc (a and d), ted (b and e), and metal oxide (c and f) of Ni(bdc)(ted)$_{0.5}$; C (brown), O (red), H (white), S (yellow), N (blue), and Ni (silver). The bond distance is in angstroms.

Table 1 Adsorption Energy (eV) of SO_2 and CO_2 in Ni(bdc)(ted)$_{0.5}$

Adsorption site	bdc	ted	Metal oxide
SO_2	−0.351	−0.469	−1.010
CO_2	−0.213	−0.307	−0.380

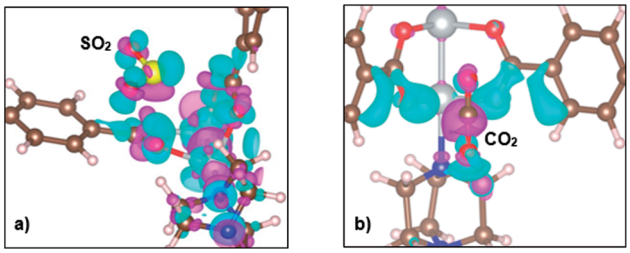

Fig. 3 The charge density difference of the most stable configuration of SO_2 (a) and CO_2 (b) found on the metal oxide. Pink and cyan clouds denote the charge loss and gain, respectively.

Table 2 Bader charges (e$^-$) of the adsorbed SO_2 and CO_2 and the MOF compared to those of the isolated ones, where (−) represents the charge loss and (+) represents the charge gain

Adsorption site	bdc	ted	Metal oxide
S	−0.013	+0.002	−0.032
2O	+0.055	+0.108	+0.102
SO_2	**+0.042**	**+0.110**	**+0.070**
20H	−0.032	−0.094	−0.005
22C	−0.005	+0.011	−0.064
2N	0.000	+0.010	−0.010
8O	−0.005	−0.032	+ 0.068
2Ni	0.000	−0.005	−0.058
MOF	**−0.042**	**−0.110**	**−0.070**
C	−0.019	−0.048	−0.066
2O	+0.036	+0.055	+0.087
CO_2	**+0.017**	**+0.008**	**+0.021**
20H	−0.019	−0.022	−0.030
22C	+0.008	+0.009	+0.005
2N	−0.002	0.000	0.000
8O	−0.003	+0.004	+0.001
2Ni	0.000	0.000	+0.003
MOF	**−0.017**	**−0.008**	**−0.021**

Table 1 shows that the adsorption strengths of both gases follow the order bdc < ted < metal oxide, which agrees with the results for SO_2 in a previous study.[13] The adsorption energy of SO_2 is significantly lower than that of CO_2 for each adsorption site, indicating that SO_2 adsorbs more strongly than CO_2. Furthermore, while the adsorption energies of CO_2 on the sites are not much different, those of SO_2 vary largely, especially on metal oxide, which implies that the metal center of Ni(bdc)(ted)$_{0.5}$ has a more significant influence on SO_2 than on CO_2.[13] A stronger binding energy of SO_2 compared with that of CO_2 at the metal site is also observed for other MOFs;[20,36,37] the binding energy of SO_2 and CO_2 at the metal oxide of Ni(bdc)(ted)$_{0.5}$ is found to be in the same order with that of Mg, Ni, and Co-MOF-74.[20] However, no comprehensive explanations based on the analysis of electronic structures have been provided for the current MOF system. Besides, vibrational energy also influences the stability of the adsorbed gases. Therefore, we calculate the vibrational frequency (ω) and the vibrational energy (1/2 $h\omega$) for the adsorbed SO_2 and CO_2. The frequencies of the three strongest vibrational modes on the metal oxide are found to be 1240, 1071, and 505 cm^{-1} for SO_2 and 2432, 1366, and 610 cm^{-1} for CO_2. For the other adsorption sites, the frequencies fluctuate around these values by less than 50 cm^{-1}. The obtained frequencies agree well with the experimental data.[13,20,38] Sequentially, the calculated vibrational energies are 0.154, 0.133, and 0.063 eV for SO_2 and 0.301, 0.169, and 0.076 eV for CO_2. The vibrational energy of the strongest SO_2 mode (0.154 eV) is significantly smaller than the adsorption energy difference (0.541 eV) between SO_2 on metal oxide and ted, whereas that of CO_2 (0.301 eV) is much higher than its adsorption energy difference (0.073 eV) between these sites. Therefore, fluctuation cannot cause transition between the most favorable adsorption sites of SO_2, but it exhibits effects on CO_2. This result implies that SO_2 is much more stable compared to CO_2 toward fluctuation.

Next, we systematically clarify the electronic structure of MOF – gas interaction. The charge density difference between SO_2 and CO_2 on the metal oxide is presented in Fig. 3a and b, respectively. The charge density difference is calculated by using eqn (2). The charge donation from SO_2 and CO_2 to MOF is depicted by the charge depletion cloud, whereas the back-donation from MOF to SO_2 and CO_2 is indicated by the

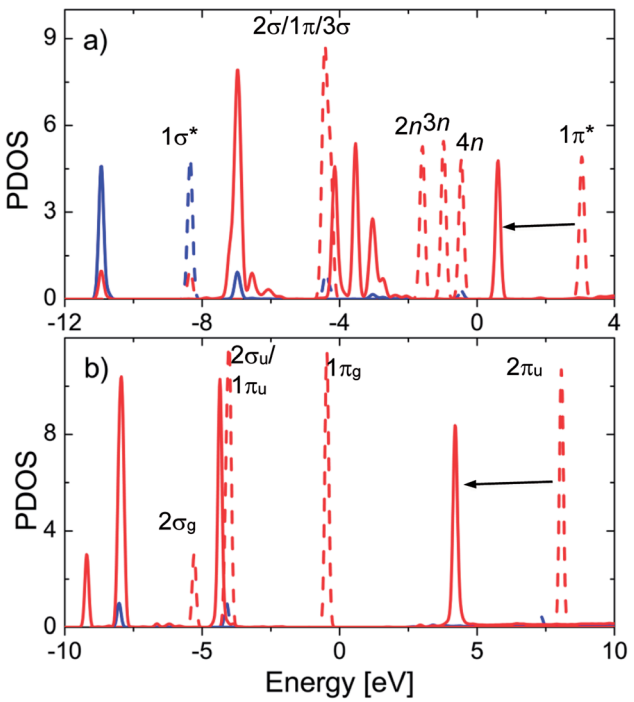

Fig. 4 The partial DOS of the isolated (dashed line) and adsorbed (solid line) gases SO_2 (a) and CO_2 (b) on the metal oxide. The s and p orbitals are presented in blue and red, respectively.

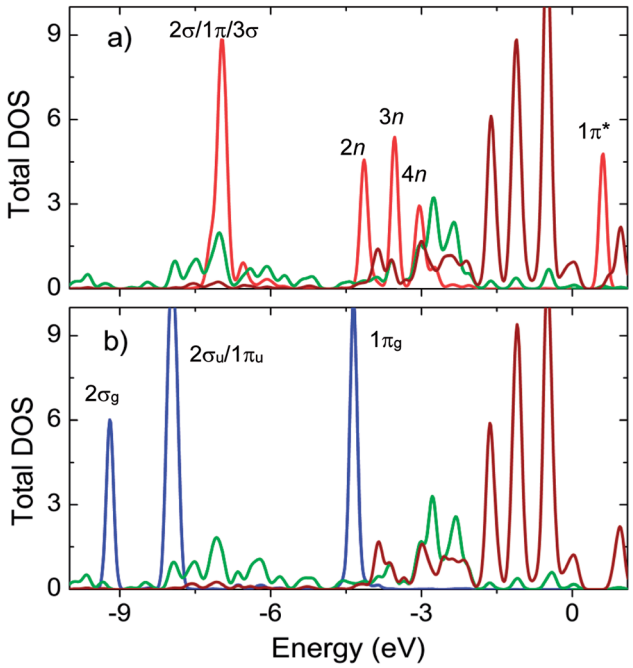

Fig. 5 The total DOS of the adsorbed SO_2 (red) and the adsorbed CO_2 (blue) on the metal oxide. The total DOS of the MOF's oxygen atoms and the d band of the Ni atoms are presented in green and brown, respectively.

charge accumulation on SO_2 and CO_2. A large extent of charge redistribution is found on Ni atoms in the case of SO_2 but not for CO_2, which is consistent with the observations from adsorption energy. The positive sign of the total point charge for the adsorbed SO_2 and CO_2 (Table 2) implies that back-donation is stronger than donation. The charge gains of the gases are mainly distributed on the oxygen atoms, and the charge gain of SO_2 is greater than that of CO_2 for all adsorption sites.

The donation of charge occurs at MOF hydrogen atoms for both SO_2 and CO_2 adsorptions and also at MOF C atoms for CO_2 adsorption for all the adsorption sites. The other MOF atoms gain or donate charge or remain neutral depending on the local sites.

Fig. 4a shows substantial expansion in the width and significant variation in the peak height of all the valence states ($2\sigma/1\pi/3\sigma$, 2n, 3n, and 4n) of SO_2. Scheme S1 and S2 in the ESI† depict the molecular orbital diagrams of SO_2 and CO_2. On the basis of these schemes, we located the peaks of electronic density of the states of SO_2 and CO_2. The modification of $2\sigma/1\pi/3\sigma$ states is mainly ascribed to (Fig. 5a) the overlap between DOS of SO_2 and that of MOF oxygen atoms, whereas the change in the 2n/3n/4n states is ascribed to the interaction of DOS of SO_2 with that of MOF oxygen atoms and the d band of Ni atoms.

Fig. 4b shows that the DOS peaks of CO_2 shifted to a lower energy level and the intensity of $2\sigma_u/1\pi_u/1\pi_g/2\pi_u$ states decreased upon adsorption, which was closely correlated to the overlap of these orbitals with those of the MOF oxygen atoms (Fig. 5b). The shift in the value of the energy level is about 2.5 eV for SO_2 and 4.0 eV for CO_2. Noticeably, there is no significant interaction between the states of CO_2 and the d band of the Ni atoms, which is entirely different from the case of SO_2. We also provide a detailed analysis of the interaction between SO_2 and CO_2 with bdc and ted in the following section.

For SO_2 on bdc, Fig. 6a shows that the peaks of DOS of SO_2 exhibit the same shape as that of isolated SO_2 with weaker

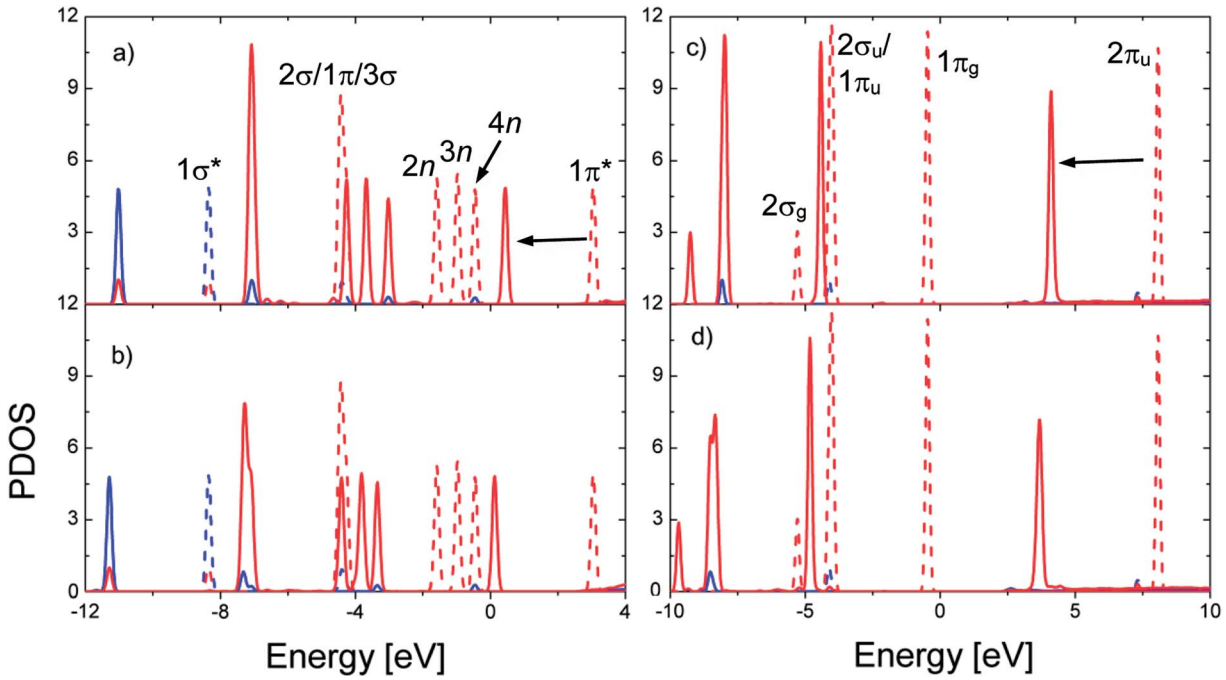

Fig. 6 The partial DOS of the adsorbed gases (solid line) and the isolated gases (dotted line) for SO_2 (left side) and CO_2 (right side): on bdc (a and c), on ted (b and d). The s and p states are presented in blue and red, respectively.

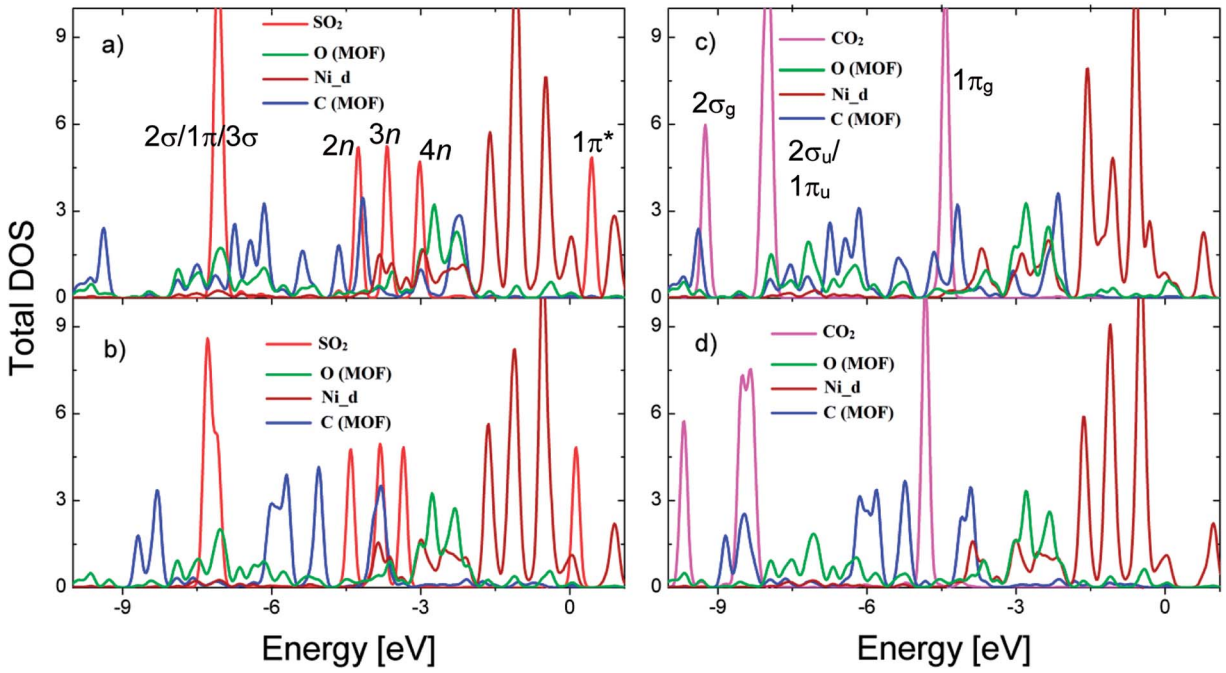

Fig. 7 The total DOS of adsorbed SO_2 (left side), adsorbed CO_2 (right side), and atoms of Ni(bdc)(ted)$_{0.5}$: on bdc (a and c), ted (b and d). The d band of the Ni atoms strongly interacts with the valence states of SO_2 but almost does not interact with the valence states of CO_2 for all the adsorption sites.

interactions between SO_2 and bdc compared with those observed on other adsorption sites. The height of the peak of $2\sigma/1\pi/3\sigma$ states is enhanced, whereas that of the 4n state is slightly reduced because of the overlap of these states with DOS of the MOF atoms (Fig. 7a). For SO_2 on ted, as presented in Fig. 6b, the width and height of $2\sigma/1\pi/3\sigma$ and 2n/3n states are modified owing to the interactions with the hydrogen and carbon atoms of ted (Fig. 7b). In particular, overlaps occur between the $2\sigma/1\pi/3\sigma$/2n states and the states of the oxygen atoms and between the 3n state and the states of the MOF carbon atoms and the d band of Ni atoms. Moreover, the $1\pi^*$ peak shifts to the Fermi level due to the overlap with the d band of Ni atoms; therefore, SO_2 gains a significantly greater charge on ted than on bdc and metal oxide (Table 2).

For CO_2, the position of the peaks shifts to a lower energy, and the height of the peaks is reduced upon adsorption (Fig. 6c and d). However, the shape of the peaks is almost unchanged except for the modification at the $2\sigma_u/1\pi_u$ states for the adsorption on ted (Fig. 6d) due to the overlap of these states with the states of ted's carbon atoms (Fig. 7d). For CO_2 on all the adsorption sites, the interaction with MOF is accomplished through the overlaps of DOS of CO_2 with DOS of the MOF C and O atoms. Noticeably, there is no significant interaction between CO_2 and the Ni atoms for all the adsorption sites, which is different from that observed for SO_2.

For the simultaneous adsorption of SO_2 and CO_2 in Ni(bdc)(ted)$_{0.5}$, we found their most favorable adsorption configurations (Fig. 8). The adsorption energies are −0.33, −0.65, and −0.41 eV for configurations (a), (b), and (c), respectively. Therefore, the configuration (b) is the most favorable one. Fig. 9 shows that the DOS of SO_2 and CO_2 show similar characteristics to those of single gas adsorption. From the above

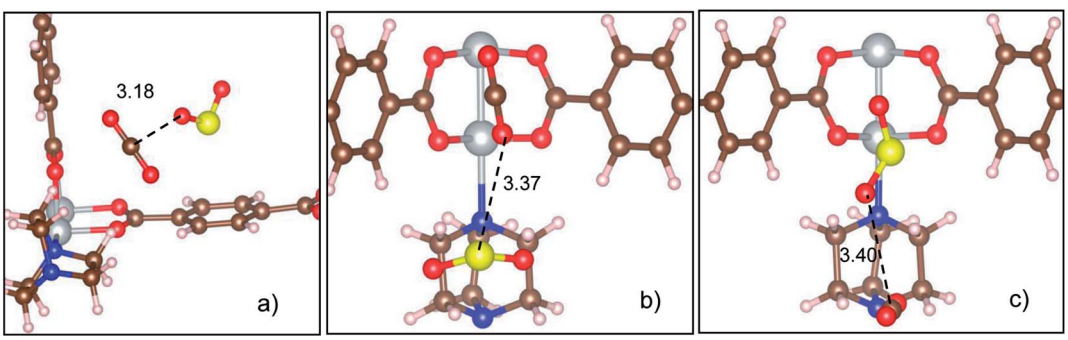

Fig. 8 The most stable configurations for co-adsorption of SO_2 and CO_2. The co-adsorption energies are −0.33, −0.65, and −0.41 eV for (a), (b), and (c), respectively; C (brown), O (red), H (white), S (yellow), N (blue), and Ni (silver). The bond distance is in angstroms.

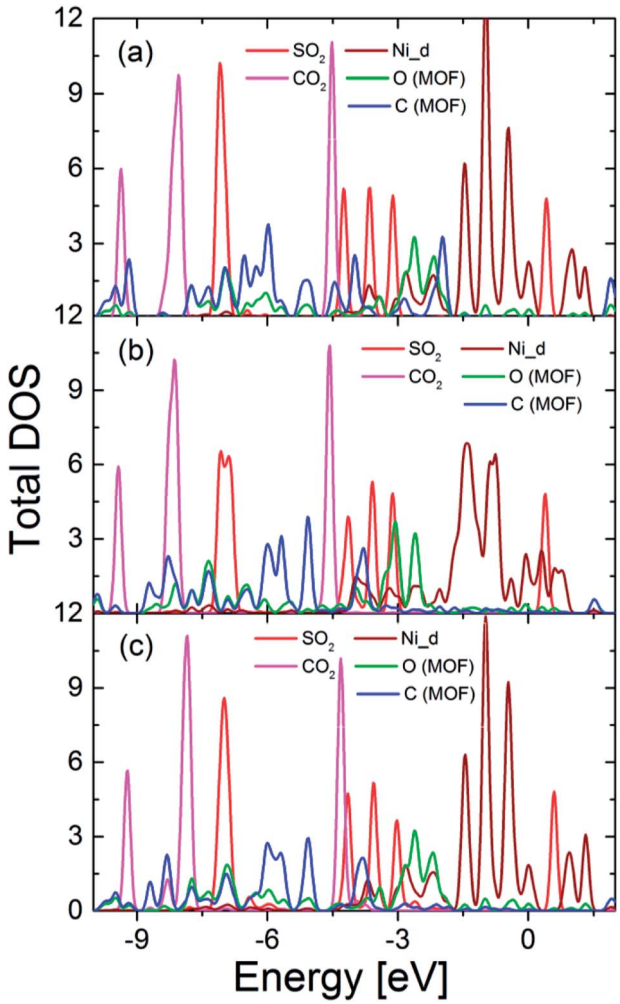

Fig. 9 The total DOS of adsorbed SO_2, adsorbed CO_2, and atoms of $Ni(bdc)(ted)_{0.5}$ for co-adsorption of SO_2 and CO_2; (a), (b), and (c) correspond to the configurations presented in Fig. 8.

analyses, we can see that while both SO_2 and CO_2 interact with the MOF C and O atoms, only SO_2 significantly interacts with Ni atoms. Thus, we can state that the participation of the d band to different extents can be the reason for competition of SO_2 and CO_2 in $Ni(bdc)(ted)_{0.5}$. Our findings support the previous experimental results about the crucial role of metal centers.[13,25] This manuscript is devoted to providing an explanation for the experimental observation regarding the co-adsorption of SO_2 and CO_2 in $Ni(bdc)(ted)_{0.5}$. Therefore, the study with different organic linkers, metal centers, and gas mixtures is beyond the scope of the present research and will be addressed[39–41] in upcoming studies.

IV. Conclusion

In conclusion, DOS of both gases homogeneously shift to lower energy levels upon adsorption. The deformations are more profound in the DOS of SO_2 than that of CO_2, including the downshifting of the anti-bonding $1\pi^*$ state of SO_2 to the Fermi level. The charge gain of SO_2 is higher than that of CO_2, which is consistent with the adsorption energy trend. Notably, the adsorption energy of SO_2 is significantly greater on metal oxide than on other adsorption sites, which is not observed in the case of CO_2, implying that the effect of Ni atoms on the adsorption of CO_2 is not much significant. This is because the d band of Ni atoms strongly interacts with the electronic states of SO_2 but does not interact with the electronic states of CO_2. The critical role of the metal center of MOFs has been addressed in the literature. Nevertheless, this study shows that this role cannot be fulfilled if the d band of the metal center does not interact with the electronic states of the adsorbed gases. We also found that increased overlap in DOS causes more charge sharing and thus stronger binding of the gas to MOF. The specific interaction between SO_2 and Ni^{2+} is unexpected since the metal ions in secondary building units of MOFs such as $M(bdc)(ted)_{0.5}$ (M is a transition metal) usually do not interact strongly with guest molecules because they are fully saturated and screened. Thus, this study presents an interesting finding, which explains the experimental result.

Conflicts of interest

There are no conflicts of interest to declare.

Acknowledgements

This research was funded by Ho Chi Minh City University of Technology – VNU-HCM under grant number T-KHUD-2017-34. We acknowledge the usage of the computer time and software granted by the Institute of Physical Chemistry of Romanian Academy, Bucharest (HPC infrastructure developed under the projects Capacities 84 Cp/I of 15.09.2007 and INFRANANOCHEM 19/01.03.2009).

References

1 T. R. Karl and K. E. Trenberth, Modern Global Climate Change, *Science*, 2003, **302**, 1719–1723.
2 G. E. Likens and F. H. Bormann, Acid Rain: A Serious Regional Environmental Problem, *Science*, 1974, **184**, 1176–1179.
3 D. Y. C. Leung, G. Caramanna and M. M. Maroto-Valer, An Overview of Current Status of Carbon Dioxide Capture and Storage Technologies, *Renewable Sustainable Energy Rev.*, 2014, **39**, 426–443.
4 K. Sumida, D. L. Rogow, J. A. Mason, T. M. McDonald, E. D. Bloch, Z. R. Herm, T.-H. Bae and J. R. Long, Carbon Dioxide Capture in Metal-Organic Frameworks, *Chem. Rev.*, 2012, **112**, 724–781.
5 D. Britt, D. Tranchemontagne and O. M. Yaghi, Metal-Organic Frameworks with High Capacity and Selectivity for Harmful Gases, *PNAS*, 2008, **105**, 11623–11627.
6 S. Yang, J. Sun, A. J. Ramirez-Cuesta, S. K. Callear, W. I. F. David, D. P. Anderson, R. Newby, A. J. Blake, J. E. Parker, C. C. Tang and M. Schröder, Selectivity and Direct Visualization of Carbon Dioxide and Sulfur Dioxide in a Decorated Porous Host, *Nature Chem.*, 2012, **4**, 887–894.

7 J.-R. Li, R. J. Kuppler and H.-C. Zhou, Selective Gas Adsorption and Seperation in Metal-Organic Frameworks, *Chem. Soc. Rev.*, 2009, **38**, 1477–1504.

8 H. Furukawa, N. Ko, Y. B. Go, N. Aratani, S. B. Choi, E. Choi, A. O. Yazaydin, R. Q. Snurr, M. O'Keeffe, J. Kim and O. M. Yaghi, Ultrahigh Porosity in Metal-Organic Frameworks, *Science*, 2010, **329**, 424–428.

9 C. Wuang, H. Liu, X. Z. Li, J. Shi, G. Ouyang, M. Peng, C. Jiang and H. N. Cui, A new concept of Desulfurization: The electrochemically Driven and Green conversion of SO_2 to $NaHSO_4$ in aqueous solution, *Environ. Sci. Technol.*, 2008, **42**, 8585–8590.

10 G. Hu, Z. Sun and H. Gao, Novel process of Simultaneous Removal of SO_2 and NO_2 by Sodium Humate Solution, *Environ. Sci. Technol.*, 2010, **44**, 6712–6717.

11 X. Y. Liu, J. M. Zhang, K. W. Xu and V. Ji, Improving SO_2 gas sensing properties of graphene by introducing dopant and defect: A first-principles study, *Appl. Surf. Sci.*, 2014, **313**, 405–410.

12 X.-D. Song, S. Wang, C. Hao and J.-S. Qiu, Investigation of SO_2 Gas Adsorption in Metal–Organic Frameworks by Molecular Simulation, *Inorg. Chem. Commun.*, 2014, **46**, 277–281.

13 K. Tan, P. Canepa, Q. Gong, J. Liu, D. H. Johnson, A. Dyevoich, P. K. Thallapally, T. Thonhauser, J. Li and Y. J. Chabal, Mechanism of Preferential Adsorption of SO_2 into Two Microporous Paddle Wheel Frameworks $M(bdc)(ted)_{0.5}$, *Chem. Mater.*, 2013, **25**, 4653–4662.

14 Z. Liang, M. Marshall and A. L. Chaffee, CO_2 adsorption selectivity and water tolerance of pillared-layer metal organic frameworks, *Microporous Mesoporous Mater.*, 2010, **132**, 305–310.

15 L. Ding and A. O. Yazaydin, The Effect of SO_2 and CO_2 Capture in Zeolitic Imidazolate Frameworks, *Phys. Chem. Chem. Phys.*, 2013, **15**, 11856–11861.

16 J. Yu, Y. Ma and P. B. Balbuena, Evaluation of the Impact of H_2O, O_2, and SO_2 on Postcombustion CO_2 Capture in Metal-Organic Frameworks, *Langmuir*, 2012, **28**, 8064–8071.

17 H.-J. Ryu, J. R. Grace and C. J. Lim, Simultaneous CO_2/SO_2 Capture Characteristics of Three Limestones in a Fluidized-Bed Reactor, *Energy Fuels*, 2006, **20**, 1621–1628.

18 T. T. T. Huong, P. N. Thanh, N. T. X. Huynh and D. N. Son, Metal – Organic Frameworks: State-of-the-art Material for Gas Capture and Storage, *VNU J. Sci.: Math. Phys.*, 2016, **32**, 67–85.

19 B. Arstad, H. Fjellvåg, K. O. Kongshaug, O. Swang and R. Blom, Amine Functionalised Metal Organic Frameworks (MOFs) as Adsorbents for Carbon Dioxide, *Adsorption*, 2008, **14**, 755–762.

20 K. Tan, S. Zuluaga, Q. Gong, Y. Gao, N. Nijem, J. Li, T. Thonhauser and Y. J. Chabal, Competitive Coadsorption of CO_2 with H_2O, NH_3, SO_2, NO, NO_2, N_2, O_2, and CH_4 in M-MOF-74 (M = Mg, Co, Ni): The Role of Hydrogen Bonding, *Chem. Mater.*, 2015, **27**, 2203–2217.

21 J. P. Perdew, K. Burke and M. Ernzerhof, Generalized Gradient Approximation Made Simple, *Phys. Rev. Lett.*, 1996, **77**, 3865–3868.

22 M. Dion, H. Rydberg, E. Schroder, D. C. Langreth and B. I. Lundqvist, Van der Waals Density Functional for General Geometries, *Phys. Rev. Lett.*, 2004, **92**(1–4), 246401.

23 P. E. Blöchl, Projector Augmented-Wave Method, *Phys. Rev. B: Condens. Matter Mater. Phys.*, 1994, **50**, 17953–17979.

24 G. Kresse and J. Joubert, From Ultrasoft Pseudopotentials to the Projector Augmented-Wave Method, *Phys. Rev. B: Condens. Matter Mater. Phys.*, 1999, **59**, 1758–1775.

25 J. Park, H. Kim, S. S. Han and Y. Jung, Tuning Metal−Organic Frameworks with Open-Metal Sites and Its Origin for Enhancing CO_2 Affinity by Metal Substitution, *J. Phys. Chem. Lett.*, 2012, **3**, 826–829.

26 H. Wu, J. M. Simmons, G. Srinivas, W. Zhou and T. Yildirim, Adsorption Sites and Binding Nature of CO_2 in Prototypical Metal−Organic Frameworks: A Combined Neutron Diffraction and First-Principles Study, *J. Phys. Chem. Lett.*, 2010, **1**, 1946–1951.

27 H. S. Koh, M. K. Rana, J. Hwang and D. J. Siegel, Thermodynamic screening of metal-substituted MOFs for carbon capture, *Phys. Chem. Chem. Phys.*, 2013, **15**, 4573–4581.

28 J. P. Perdew, J. A. Chevary, S. H. Vosko, K. A. Jackson, M. R. Pederson, D. J. Singh and C. Fiolhais, Atoms, Molecules, Solids, and Surfaces: Applications of the Generalized Gradient Approximation for Exchange and Correlation, *Phys. Rev. B: Condens. Matter Mater. Phys.*, 1992, **46**, 6671–6687.

29 D. C. Langreth, B. I. Lundqvist, S. D. Chakarova-Käck, V. R. Cooper, M. Dion, P. Hyldgaard, A. Kelkkanen, J. Kleis, L. Kong, S. Li, P. G. Moses, E. Murray, A. Puzder, H. Rydberg, E. Schröder and T. Thonhauser, A Density Functional for Sparse Matter, *J. Phys.: Condens. Matter*, 2009, **21**(1–15), 084201.

30 H. J. Monkhorst and J. D. Pack, Special Points for Brillouin-Zone Integrations, *Phys. Rev. B: Condens. Matter Mater. Phys.*, 1976, **13**, 5188–5192.

31 G. Rojas, S. Simpson, X. Chen, D. A. Kunkel, J. Nitz, J. Xiao, P. A. Dowben, E. Zurek and A. Enders, Surface State Engineering of Molecule–molecule Interactions, *Phys. Chem. Chem. Phys.*, 2012, **14**, 4971–4976.

32 W. G. Schmidt, K. Seino, M. Preuss, A. Hermann, F. Ortmann and F. Bechstedt, Organic Molecule Adsorption on Solid Surfaces: Chemical Bonding, Mutual Polarisation and Dispersion Interaction, *Appl. Phys. A*, 2006, **85**, 387–397.

33 D. N. Son, O. K. Le, M. T. Hiep and V. Chihaia, Magnetic anisotropy of ultrathin $Pd_4Co(111)$ film by first-principles calculations, *J. Sci.: Adv. Mat. Dev.*, 2018, **3**, 243–253.

34 G. Henkelman, A. Arnaldsson and H. Jonsson, A Fast and Robust Algorithm for Bader Decomposition of Charge Density, *Comput. Mater. Sci.*, 2006, **36**, 354–360.

35 N. T. X. Huynh, O. M. Na, V. Chihaia and D. N. Son, A computational approach towards understanding hydrogen gas adsorption in Co-MIL-88A, *RSC Adv.*, 2017, **7**, 39583–39593.

36 K. Yu, K. Kiesling and J. R. Schmidt, Trace Flue Gas Contaminants Poison Coordinatively Unsaturated Metal-

Organic Frameworks: Implications for CO_2 Adsorption and Separation, *J. Phys. Chem. C*, 2012, **116**, 20480–20488.

37 L. Ding and A. Ö. Yazaydin, How Well Do Metal–Organic Frameworks Tolerate Flue Gas Impurities?, *J. Phys. Chem. C*, 2012, **116**, 22987–22991.

38 V. Wathelet, B. Champagne, D. H. Mosley, E. A. Perpète and J. M. André, Vibrational Frequencies of H_2O and CO_2 from Car-Parrinello Molecular Dynamics, *J. Mol. Struct.: THEOCHEM*, 1998, **425**, 95–100.

39 L. Du, Z. Lu, L. Xu and J. Zhang, A new mfj-type metal–organic framework constructed from a methoxyl derived V-shaped ligand and its H_2, CO_2 and CH_4 adsorption properties, *RSC Adv.*, 2017, **7**, 21268–21272.

40 C. Altintas and S. Keskin, Molecular simulations of MOF membranes for separation of ethane/ethene and ethane/methane mixtures, *RSC Adv.*, 2017, **7**, 52283–52295.

41 F. Zhou, J. Zhou, X. Gao, C. Kong and L. Chen, Facile synthesis of MOFs with uncoordinated carboxyl groups for selective CO_2 capture via postsynthetic covalent modification, *RSC Adv.*, 2017, **7**, 3713–3719.